Molecules and Cells

Structure and Function of the Autolysin SagA in the Type IV Secretion System of *Brucella abortus*

Yongseong Hyun, Yeongjin Baek, Chanyoung Lee, Nayeon Ki, Jinsook Ahn, Sangryeol Ryu, and Nam-Chul Ha*

Department of Agricultural Biotechnology, Research Institute for Agriculture and Life Sciences, Center for Food and Bioconvergence, CALS, Seoul National University, Seoul 08826, Korea
*Correspondence: hanc210@snu.ac.kr
https://doi.org/10.14348/molcells.2021.0011
www.molcells.org

A recent genetic study with *Brucella abortus* revealed the secretion activator gene A (SagA) as an autolysin component creating pores in the peptidoglycan (PGN) layer for the type IV secretion system (T4SS) and peptidoglycan hydrolase inhibitor A (PhiA) as an inhibitor of SagA. In this study, we determined the crystal structures of both SagA and PhiA. Notably, the SagA structure contained a PGN fragment in a space between the N- and C-terminal domains, showing the substrate-dependent hinge motion of the domains. The purified SagA fully hydrolyzed the meso-diaminopimelic acid (DAP)-type PGN, showing a higher activity than hen egg-white lysozyme. The PhiA protein exhibiting tetrameric assembly failed to inhibit SagA activity in our experiments. Our findings provide implications for the molecular basis of the SagA-PhiA system of *B. abortus*. The development of inhibitors of SagA would further contribute to controlling brucellosis by attenuating the function of T4SS, the major virulence factor of *Brucella*.

Keywords: autolysin, *Brucella abortus*, meso-diaminopimelic acid, muramidase, type IV secretion system

INTRODUCTION

The three-dimensional mesh-like structure of peptidoglycan (PGN) creates robust physical properties for bacterial survival. The linear backbone chains of alternating *N*-acetylglucosamine (GlcNAc) and *N*-acetylmuramic acid (MurNAc) are interconnected by stem peptides (Koraimann, 2003). PGN can be expanded and turned over due to muramidase cutting the backbone sugar chains. The immune systems of mammals and invertebrates have PGN-degrading enzymes, such as lysozyme, that efficiently kill invading bacteria as front-line defense weapons.

Gram-negative bacteria have six protein secretion systems, spanning the inner membrane, periplasm, and outer membrane in the typical cell envelope structure of Gram-negative bacteria (Alvarez-Martinez and Christie, 2009; Hueck, 1998; Kanonenberg et al., 2013; Korotkov et al., 2012; Lasica et al., 2017; Pukatzki et al., 2009). The physical barrier of the PGN layer hinders the assembly of multicomponent secretory systems. Most secretion systems have a lytic transglycosylase component, called autolysin, to create a pore in the PGN layer, allowing the large multicomponent complex to pass through (Dijkstra and Keck, 1996). The local degradation of the PGN layer by autolysin is also involved in creating pores for the insertion of flagella (Scheurwater et al., 2008). However, unregulated autolysin could damage bacteria since the PGN layer is critical for the mechanical support of bacterial cells.

Brucella abortus is a facultative intracellular pathogenic bacterium causing brucellosis in both humans and cattle (Pappas et al., 2006). Humans suffer from recurrent fever

Received 15 January, 2021 ; revised 17 February, 2021; accepted 17 February, 2021; published online 11 June, 2021

eISSN: 0219-1032

and debilitating musculoskeletal, cardiac, and neurological complications during the chronic stage of brucellosis (Archambaud et al., 2010). *B. abortus* produces and secretes several effector proteins to survive in host immune cells (Myeni et al., 2013). A recent study discovered secretion activator gene A (SagA) in *B. abortus*, together with its proteinaceous inhibitor peptidoglycan hydrolase inhibitor A (PhiA) (Del Giudice et al., 2013; 2019). SagA is the pore-forming autolysin in the type IV VirB system and responsible for preventing the fusion of *Brucella*-containing vacuoles (BCVs) with lysosomes of immune cells. SagA is homologous to typhoid toxin secretion A (TtsA), which was recently determined an autolysin in the toxin translocation system of *Salmonella* (Hodak and Galan, 2013). Both SagA and TtsA are dissimilar from mammalian lysozymes exhibiting the same muramidase activity (Del Giudice et al., 2013). Since SagA is involved in the early stages of intracellular replication of *B. abortus*, SagA may be a target for the treatment of brucellosis.

The crystal structure of TtsA from *Salmonella enterica* serovar Typhimurium (*S.* Typhimurium, *St*TtsA) was determined in complex with *meso*-diaminopimelic acid (DAP), revealing the overall clamp-like shape. DAP is found in the stem peptide in the PGN for linking the stem peptides in most Gram-negative bacterial PGN and *Bacillus* sp. in Gram-positive bacteria. Instead of DAP, Lys is found in most Gram-positive bacteria. A previous study proposed reaction and substrate recognition mechanisms highlighting the bound DAP molecule (Geiger et al., 2020). However, the catalytic mechanism and substrate-binding mode remained elucidated since the structure did not contain the substrate PGN. Here, we report the crystal structure of SagA in complex with a PGN repeating unit demonstrating the substrate-binding site, providing functional implications in the SagA system. The crystal structure and functional implications of PhiA are also studied.

MATERIALS AND METHODS

Protein expression and purification of SagA and PhiA

The *sagA* gene sequence without the transmembrane region (residues 1-174, SagAΔTM) and *phiA* gene was synthesized after codon optimization for *Escherichia coli* expression (Bioneer, Korea) (Puigbo et al., 2007). Then, the DNA molecule encoding SagAΔTM or PhiA was inserted into the expression vector pET28a using the restriction enzyme sites *Nco*I and *Xho*I (Hyun et al., 2020). The resulting pET28a-SagAΔTM and pET28a-PhiA FL vectors contained the hexa-histidine tag at the C-terminus of the protein. The procedures for the protein expression and purification of SagAΔTM were previously reported (Hyun et al., 2020). Briefly, *E. coli* BL21 (DE3) cells harboring the resulting plasmid were cultured in LB broth and disrupted by sonication. For selenomethionine (SeMet)-labeled SagAΔTM, *E. coli* B834 (DE3) was cultured in M9 medium supplemented with L-selenomethionine. The cell lysate was mixed with Ni-NTA agarose resin (1 ml; Qiagen, Germany) in lysis buffer containing 20 mM Tris (pH 8.0), 150 mM NaCl, and 2 mM β-mercaptoethanol. After washing with buffer containing 20 mM imidazole, the protein was eluted with buffer containing 250 mM imidazole (pH 8.0). The proteins were further purified on a gel filtration chromatographic column (HiLoad™ 26/610 Superdex™ 200 pg; GE Healthcare, USA) in lysis buffer. For PhiA, the proteins were further purified using anion-exchange chromatography (HiTrap Q; GE Healthcare) before application to the gel filtration chromatography column. The proteins were concentrated using Vivaspin (Millipore, USA) to 15 mg/ml for SagA and to 12 mg/ml for PhiA.

Crystallization, data collection, and processing

The crystallization conditions were optimized using the hanging-drop diffusion method at 14°C. SagA was crystallized in solution containing 0.2 M ammonium acetate, 0.1 M sodium acetate trihydrate (pH 4.1), 21% (w/v) polyethylene glycol 4,000, and 2 mM Tris (2-chloroethyl) phosphate (TCEP). SeMet-labeled SagA was a crystallized solution containing 0.1 M sodium citrate (pH 5.5), and 27% (v/v) Jeffamine ED-2001. PhiA protein was crystallized in solution containing 0.1 M BIS-Tris (pH 6.0), and 18% (w/v) PEG 10,000. For data collection under cryogenic conditions, SagAΔTM crystals were transferred to 2 μl of the viscous oil Paraton-N and incubated for 1 s. Then, the crystals were flash-cooled in liquid nitrogen at −196°C. The datasets were collected using an Eiger 9M detector (Dectris, Switzerland) at a wavelength of 1.00003 Å in beamline 5C and a Pilatus 3-6M detector (Dectris) at a wavelength of 0.97942 Å in beamline 11C of the Pohang Accelerator Laboratory, Republic of Korea. The diffraction datasets were processed, merged, and scaled using the program HKL-2000 (Otwinowski and Minor, 1997). Table 1 shows the data collection statistics.

Structural determination

For SagA, the initial model was built on phase information from the SAD dataset for SeMet-labeled crystals at 2.7 Å resolution (Terwilliger et al., 2009). The structure was refined against the 2.0 Å resolution native dataset. The structure of PhiA was determined using the molecular replacement method using Phenix Phaser-MR software (McCoy et al., 2007). All of the structures were built using COOT and refined using Phenix.refine software (Adams et al., 2010; Emsley and Cowtan, 2004). The detailed refinement statistics are shown in Table 1.

Muramidase activity assay

All assays were performed using a UV-visible spectrophotometer, Multiscan Go (Thermo Fisher Scientific, USA). The activity of SagA and hen egg-white lysozyme (HEWL) (L6876; Sigma-Aldrich, USA) was measured using freeze-dried *Micrococcus lysodeikticus* cells (ATCC4698; Sigma-Aldrich) and *Bacillus subtilis* cells (ATCC6633) suspended in 20 mM potassium phosphate buffer (pH 7.0). Kinetics were determined by optical density at 600 nm at 25°C, and reaction rates were calculated based on the change in absorbance per minute (ΔOD_{600}/min). SagA and lysozyme were treated at a final concentration of 100 nM.

To examine the product inhibition of SagA, we generated a reaction product of *M. lysodeikticus* cells hydrolyzed by HEWL. *M. lysodeikticus* cells were suspended in 20 mM of potassium phosphate buffer (pH 7.0) at a concentration of 5 mg/ml and treated with HEWL at a final concentration of

Table 1. Data collection and refinement statistics

	Native SagA	SeMet SagA	PhiA
Data collection			
Beamline	PAL 5C	PAL-11C	PAL-11C
Wavelength (Å)	1.00003	0.97942	0.97942
Space group	$P2_13$	$P2_13$	$P2_12_12$
Cell dimensions			
a, *b*, *c* (Å)	79.04	79.40	66.16, 51.16, 62.30
Resolution (Å)	50.00-2.00 (2.03-2.00)	50.00-2.70 (2.75-2.70)	50.00-1.80 (1.83-1.80)
Total No. reflections	11,424	4,744	19,949
R_{merge}	0.049 (0.239)	0.179 (0.426)	0.092 (0.311)
Highest resolution shell CC1/2	0.989	0.873	0.953
I/σ (I)	67.5 (15.6)	19.3 (8.5)	23.7 (5.3)
Completeness (%)	100.0 (99.8)	100.0 (99.6)	99.0 (97.1)
Redundancy	30.7 (23.4)	22.6 (13.6)	9.7 (6.2)
Refinement statistics			
Resolution (Å)	45.63-2.00		45.36-1.80
No. of reflections	11,405		19,837
R_{work}/R_{free}	0.1860/0.2243		0.1992/0.2309
No. of total atoms	1,431		1,511
Wilson B-factor (Å^2)	23.35		17.16
RMSD			
Bond lengths (Å)	0.003		0.007
Bond angles (°)	0.53		0.951
Ramachandran plot			
Favored (%)	99.42		96.53
Allowed (%)	0.58		3.47
Outliers (%)	0		0
PDB ID	7DNP		7DPY

$R_{merge} = \Sigma_{hkl}\Sigma_i|I_i(hkl) - [I(hkl)]|/\Sigma_{hkl}\Sigma_i I_i(hkl)$, where $I_i(hkl)$ is the intensity of the *i*th observation of reflection *hkl* and [I(*hkl*)] is the average intensity of *i* observations.

1 μM for 1 h at 37°C. After complete digestion by HEWL, the samples were heat-treated at 100°C for 1 h to inactivate the remaining proteins. The sample was then centrifuged at 10,000*g*, and the supernatant was used as the reaction product of muramidase. In the experiment examining the product-inhibition mode, 20 μl of the product was added to a 200 μl reaction of *M. lysodeikticus* cells by SagA or HEWL.

To observe the effect of DAP on the activity of SagA, we added 2,6-diaminopimelic acid (Sigma-Aldrich) to the reaction mixture. SagA (500 nM) or HEWL (500 nM) was added to *M. lysodeikticus* cells or *B. subtilis* cells in the presence or absence of 5 mM DAP.

Quantification of bacterial survival

Quantification of the viability of bacteria in SagA- or HEWL-treated samples was measured by the colony counting method. Freeze-dried *M. lysodeikticus* cells were suspended in 20 mM potassium phosphate buffer (pH 7.0) at a concentration of 0.1 mg/ml. Then, we treated SagA and HEWL at a final concentration of 50 nM for 1 h. After treatment, decimal dilution was performed in the same buffer and seeded onto LB agar plates. Colonies were counted after 48 h of incubation at 37°C.

Statistical analysis

All data are presented as mean ± SD. The values were obtained from at least three repetitive experiments. The experiment results were determined by applying the unpaired *t*-test using GraphPad Prism version 8.0.1 (GraphPad Software Inc., USA). Significance of analysis is indicated in the figures (ns: not significant, $*P < 0.05$, $****P < 0.0001$).

N-terminal amino acid sequencing

The purified PhiA protein was subjected to SDS-PAGE and electrically transferred onto a polyvinylidene fluoride (PVDF) membrane (Westran Clear Signal; GE Healthcare). After staining with Coomassie Brilliant Blue-R-250 staining solution, the detected band was analyzed by the Edman degradation protein sequencing service (EMASS, Korea).

Size exclusion chromatography coupled with multiangle light scattering (SEC-MALS)

Each sample was subjected to size exclusion chromatography (SEC) on a Superdex 200 increase 10/300 GL column (GE Healthcare). The molecular sizes and oligomerization states of PhiA were measured by MALS (DAWN HELIOS II; Wyatt Technology, USA).

Accession numbers

The atomic coordinates and structure factors (codes 7DNP and 7DPY) have been deposited in the Protein Data Bank (PDB; http://wwpdb.org/).

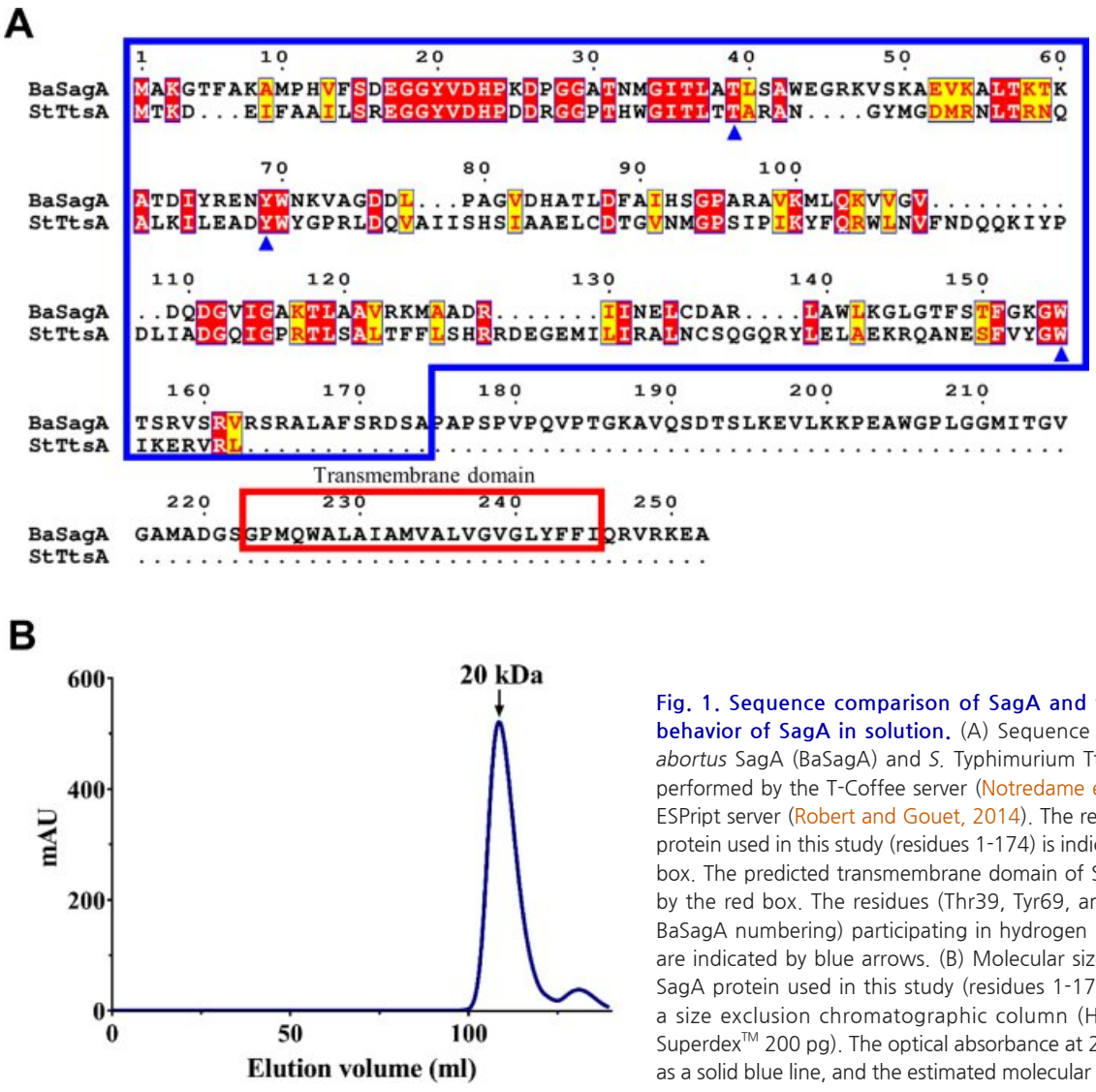

Fig. 1. Sequence comparison of SagA and the monomeric behavior of SagA in solution. (A) Sequence alignment of *B. abortus* SagA (BaSagA) and *S.* Typhimurium TtsA (StTtsA) was performed by the T-Coffee server (Notredame et al., 2000) and ESPript server (Robert and Gouet, 2014). The recombinant SagA protein used in this study (residues 1-174) is indicated by the blue box. The predicted transmembrane domain of SagA is indicated by the red box. The residues (Thr39, Tyr69, and Trp155 in the BaSagA numbering) participating in hydrogen bonds with PGN are indicated by blue arrows. (B) Molecular size of the purified SagA protein used in this study (residues 1-174), measured by a size exclusion chromatographic column (HiLoad™ 26/610 Superdex™ 200 pg). The optical absorbance at 280 nm is plotted as a solid blue line, and the estimated molecular size is indicated.

RESULTS

Structural determination and overall structure of SagA

The recombinant SagA protein, deleted in the C-terminal transmembrane region (hereafter called SagA), was cytosolically produced in the *E. coli* expression system (Fig. 1A). The monomeric protein in the solution was crystallized using the hanging drop method, as previously described (Fig. 1B) (Hyun et al., 2020). The data collection of flash-frozen crystals was collected and produced a dataset that featured 99.8% completeness at 2.0 Å resolution (Table 1). The crystal structure of SagA was determined by the single anomalous dispersion method using anomalous signals from selenomethionine in the crystals.

The overall structure of SagA is similar to that of *St*TtsA, consisting of two domains connected by a linker. The crystal structure revealed that SagA has two α-helical domains: an N-terminal domain (residues 1-73; cyan in Fig. 2A) and a C-terminal domain (residues 82-174; pink in Fig. 2A), hinged by a short helix and loops (residues 74-81; orange in Fig. 2A). These structural arrangements are similar to that of T4 lysozyme, consisting of the two domains that are connected by a long helix (Matthews and Remington, 1974). The N-terminal domains of SagA and *St*TtsA have a high sequence similarity to the N-terminal hydrolase domain of T4 lysozyme, including the catalytic residues (Glu17, Asp26, and Thr31 in the SagA numbering). The N-terminal hydrolase domains of SagA and *St*TtsA consist of four α-helices (α1-α4) and a long flexible loop (α1-α2 loop; residues 17-37) connecting α1 and α2. The long flexible loop in the N-terminal domain contains conserved catalytic residues. The C-terminal domain of SagA forms a compact α-helical bundle with five α-helices (α5-α9) that show structural and sequence similarity to the PGN binding domain of *St*TtsA.

As previously observed in the *St*TtsA and T4 lysozyme structures (Geiger et al., 2020; Kuroki et al., 1993), the putative substrate-binding site of SagA is located in a space between the N-terminal and the C-terminal domains. The

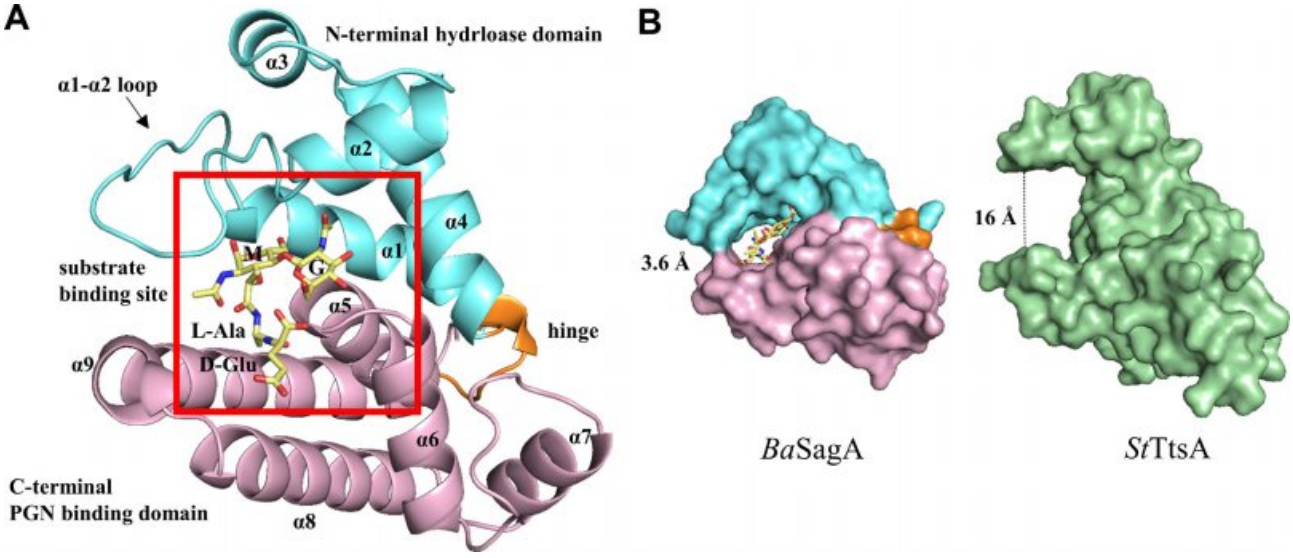

Fig. 2. The overall structure of SagA and the substrate-induced conformational change. (A) Crystal structure of the SagA protein as shown by ribbon representations. The N-terminal hydrolase domain (cyan), hinge (orange), and C-terminal PGN binding domain (pink) are labeled. The secondary structural elements of SagA are labeled. The substrate-binding site is indicated by the red box. "α1-α2 loop" stands for the loop connecting α1 and α2. MurNAc (M), GlcNAc (G), L-Ala, and D-Glu of the PGN repeating unit (yellow) in the substrate-binding site are shown in stick model. (B) Difference in the opening of the substrate-binding site of *Ba*SagA from *St*TtsA. The surface representations of *B. abortus* SagA (left, *Ba*SagA) and *S.* Typhimurium TtsA (right, *St*TtsA, PDB ID: 6V40) are depicted. The nearest distance between the α1-α2 loop and the C-terminal domain is indicated.

substrate-binding site is lined with the α1-α2 loop of the N-terminal domain and the beginning of α9 in the C-terminal domain (Fig. 2A). The closest distances between the α1-α2 loop (residue 26) and the beginning of α9 (residue 151) are 3.6 Å in the SagA structure. The corresponding region is separated by 7-16 Å in the *St*TtsA structures (Fig. 2B). Thus, the clamping region of SagA is closer than that of the *St*TtsA structure (Geiger et al., 2020). These findings suggest high structural plasticity between the N-terminal flap domain and the C-terminal domain, presumably resulting in the spatial adjustment of the substrate-binding site.

The substrate-binding site of SagA

We found an extra electron density map at the putative substrate-binding site of SagA, which enabled us to build a part of the PGN repeating unit (GlcNAc-MurNAc-L-Ala-D-Glu) (Fig. 3A). The PGN repeating unit in SagA seemed to be from a digested product of *E. coli* cell wall components during purification. The GlcNAc moiety at the nonreducing end of the PGN backbone is deep inside the substrate-binding site between the N- and C-terminal domains. The acetyl group at C2 and the hydroxyl group at C3 of GlcNAc make hydrogen bonds with the side chains of Thr39 (in α2) and Tyr69 (in α4) in the N-terminal flap domain (Fig. 3B). The acetyl group also makes hydrophobic interactions with Ile35 in the α1-α2 loop and Tyr65 in α4 in the N-terminal flap domain. Thus, the acetyl group may be necessary for binding to the SagA substrate-binding site.

The α1-α2 loop and α1 in the N-terminal domain surround the MurNAc moiety in the PGN backbone. The α5, α8, and α9 in the C-terminal domain also interact with the MurNAc moiety (Fig. 3B). The acetyl group of MurNAc forms hydrogen bonds in a space between the N-terminal and C-terminal domains with the side chain of His92 in α5 and Trp155 in α9, together with hydrophobic interactions with Phe151 in α9. His92 corresponds to the Asn/Gln residue of the Pho-Asn/Gln motif (Pho indicates hydrophobic residues), which is an essential motif for hydrogen-bond interactions with PGN in the T4 lysozyme family (Pei and Grishin, 2005). Thr39, Tyr69, and Trp155 residues in the binding of the acetyl groups in PGN are conserved in *St*TtsA and the family of *N*-acetylmuramidases (Fig. 1A) (Stojkovic and Rothman-Denes, 2007). This finding suggests that the substrate recognition mechanisms are shared with *St*TtsA and other *N*-acetylmuramidase family proteins.

We next examined the stem peptide moiety attached to the C3 atom of MurNAc in the crystal structure of SagA. L-Ala and D-Glu in the stem peptide did not form specific polar interactions with the SagA residues. Only van der Waals interactions were found near Leu142 and Leu145 of α8 in the C-terminal domain (Figs. 3A and 3B). Our findings indicate that the acetyl moieties at C2 of GlcNAc and at C2 of MurNAc may contribute to recognizing PGN by SagA rather than stem peptides.

According to the proposed mechanism for T4 lysozyme (Kuroki et al., 1999), a water molecule hydrogen-bonded to Asp20 and Thr26 acted as the nucleophile, attacking the C1 atom of MurNAc. Glu11 of T4 lysozyme, on the opposite side of Asp20 and Thr26, was presumed to act as a proton donor to oxygen O1 of MurNAc (Fig. 3C). The crystal structure of SagA revealed the corresponding and conserved Glu, Asp, and Thr residues (Glu17, Asp26, and Thr31 in the SagA

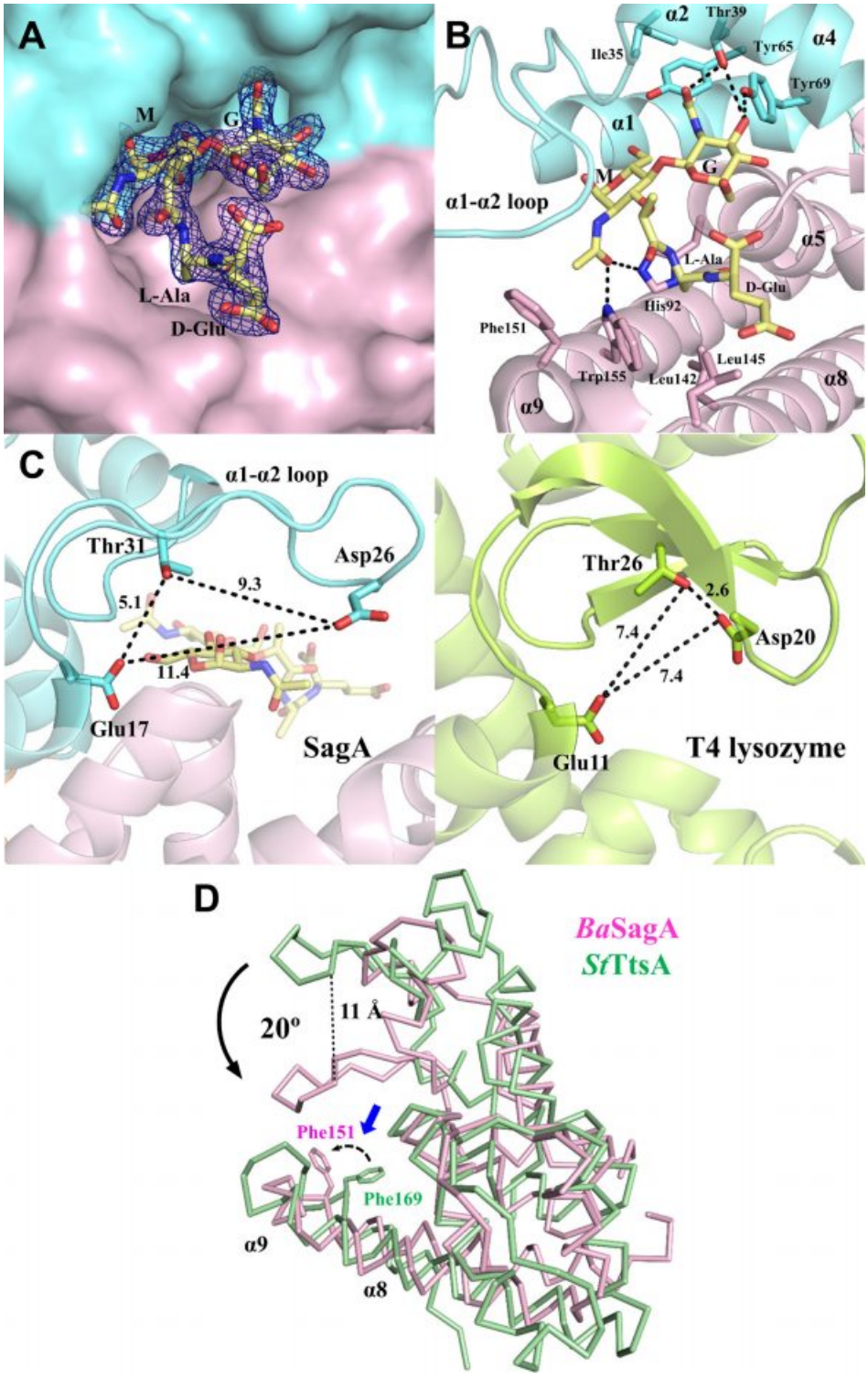

Fig. 3. PGN binding in the substrate-binding site of SagA and structural comparison with T4 lysozyme and *St*TtsA. (A) Electron density map indicating the MurNAc (M), GlcNAc (G), L-Ala, and D-Glu of the PGN repeating unit (yellow) in the substrate-binding site. The PGN repeating unit is shown in the stick model, and the SagA is in the surface representation. The electron density maps (2FoFc) are depicted in the blue mesh contoured at 1.0 σ. (B) Amino acid residues involved in the interactions with PGN. The PGN repeating unit (yellow) and amino acid residues (cyan; Ile35, Thr39, Tyr65, and Tyr69, pink; His92, Leu142, Leu145, Phe151, and Trp155) are shown in the stick model. The hydrogen bonds are indicated by the dotted lines. (C) Comparison of the catalytic residues of SagA and T4 lysozyme. The catalytic residues of SagA (Glu17, Asp26, and Thr31) are shown as stick models in the left panel. The catalytic residues (Glu11, Asp20, and Thr26) of T4 lysozyme (PDB ID: 1L02) are shown as stick models in the right panel. (D) The structural superposition of *Ba*SagA (pink) and *St*TtsA (green) with the reference of the C-terminal domains is shown in the ribbon representations. The motion of the N-terminal domain with the reference of the C-terminal domain is indicated by an arrow. The distance between the N-terminal domains of *Ba*SagA and *St*TtsA is indicated. The turn region between α8 and α9 of the C-terminal domain is indicated by the blue arrow. Phe151 of *Ba*SagA (pink) and Phe169 of *St*TtsA (green) are shown in the stick model. PGN-induced conformational changes in Phe are indicated by dotted arrows.

numbering) in the active site, suggesting that T4 lysozyme and SagA share the same reaction mechanism. However, the Glu17 residue of SagA is too far to attack the oxygen atom of MurNAc, and the Asp26 and Thr31 residues of SagA are not within distance to make hydrogen bonds with the water molecule. Thus, our structure suggests that local conformational change of the α1-α2 loop in crystal structure of SagA to close the Asp26 residue toward the Thr31 residue may be necessary for catalysis.

PGN-induced clamping motion

We compared the SagA structure in complex with a part of

the PGN repeating unit to the *St*TtsA structure that contains only a DAP molecule. The structural superpositions between individual N-terminal domains or the C-terminal domains of SagA and *St*TtsA are well aligned (the root-mean-square-deviation [RMSD] between 44 and 47 matched Cα atoms are 0.9 Å and 2.4 Å, respectively). However, a substantial hinge

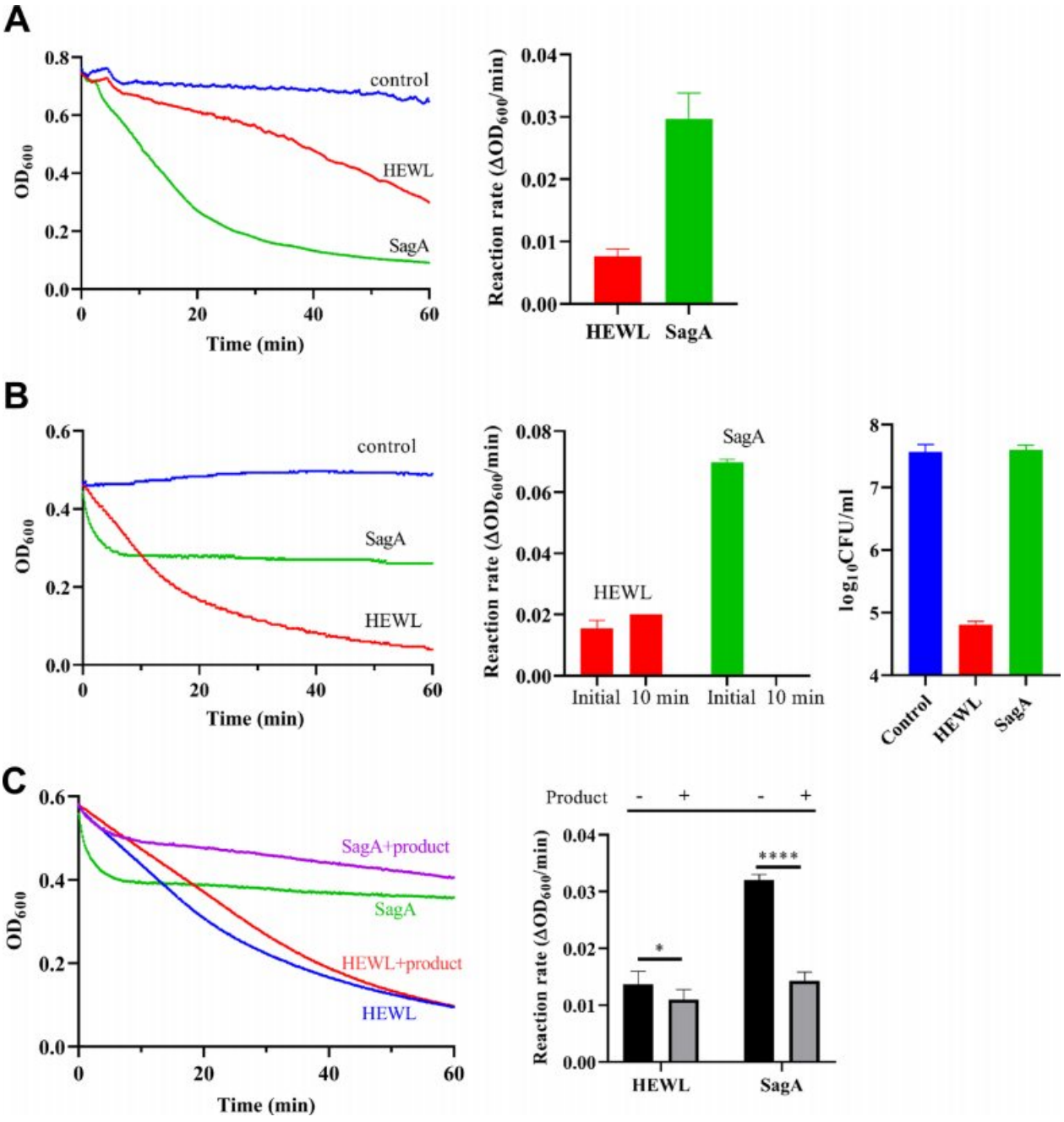

Fig. 4. Muramidase activity of SagA. (A) Turbidimetric changes in HEWL- or SagA-treated *B. subtilis* cells (left panel; 100 nM proteins were used). The right panel shows the initial reaction rates of the turbidimetric changes (left panel) from three independent experiments. Values are presented as mean ± SD. (B) Turbidimetric changes in HEWL- or SagA-treated *M. lysodeikticus* cells (left panel; 100 nM proteins were used). The middle panel presents the initial reaction rates (initial) and the intermediate reaction rates in 10 min (10 min) of the turbidimetric changes (left panel). The right panel shows the colony-forming units (CFUs) of HEWL- or SagA-treated *M. lysodeikticus* cells. These results were produced from three independent experiments. Values are presented as mean ± SD. (C) Product-inhibited reaction of SagA in *M. lysodeikticus* cells. The left panel presents the turbidimetric changes in HEWL- or SagA-treated *M. lysodeikticus* cells in the presence and absence of the reaction product. The right panel presents the initial reaction rates of HEWL and SagA of the turbidimetric changes from the three independent experiments. Values are presented as mean ± SD. $*P < 0.05$, $****P < 0.0001$.

motion was found between the N-terminal and C-terminal domains (Fig. 3D). Approximately 11 Å motion (Cα of Gly28 of SagA and Gly25 of *St*TtsA) and 20° rotation of the N-terminal domain were measured when the structures were superposed using the C-terminal domains as the reference. The hinge motion is comparable to the "clamping" of the substrate-binding region. Structural comparison to *St*TtsA suggested that the clamping is coupled with PGN binding to the substrate-binding site of SagA, which is represented by the induced-fit model of the enzymes (Fig. 2B).

We found another conformational change induced by PGN binding in the turn region between α8 and α9 of the C-terminal domain (blue arrow in Fig. 3D). The phenyl ring of Phe151 of SagA is inward to the clamping area by hydrophobic interaction with the acetyl group in MurNAc of PGN. In contrast, the corresponding Phe169 of *St*TtsA is outward from the clamping area. PGN binding causes conformational changes in the C-terminal domain and clamping motion between the two domains.

Muramidase activities of SagA

We compared the muramidase activities of SagA and hen egg-white lysozyme (HEWL) using *B. subtilis* cells as DAP-type PGNs. The activities, evaluated by the reduced rate of cellular turbidity, showed a threefold higher muramidase activity of SagA than that of HEWL (Fig. 4A). In a similar experiment with *M. lysodeikticus* cells for Lys-type PGN, SagA also exhibited a higher activity than HEWL at the initial stage (within ~5 min). However, the activity of SagA sharply decreased after 5 min, resulting in only partial digestion of the cells, unlike HEWL (Fig. 4B). As expected, the SagA treatment could not kill the bacteria with only partial digestion of the bacterial cells, which was different from the 3-log reduction by the HEWL treatment (Fig. 4B).

To investigate the mechanistic reason for the limited activity of SagA on Lys-type PGN, we first suspected depletion of the substrates or the active SagA during the enzyme reaction. The supplementation of the substrate cells or the enzyme SagA in the middle of the reaction with SagA did not affect the reaction rate (Supplementary Fig. S1). However, in the case of HEWL, the addition of the substrate cells or the HEWL enzyme increased the reaction rates. When we added the reaction product of *M. lysodeikticus* cells by HEWL to the reaction mixture of the cells, the reaction rate of SagA was severely decreased, unlike that of HEWL (Fig. 4C). These observations indicate that the reaction product of muramidase strongly inhibits the activity of SagA. We next tested whether SagA could degrade *O*-acetylated PGNs, such as from *Staphylococcus aureus* and *Bacillus cereus*. The *O*-acetylated PGNs normally show the resistance to lysozymes. The results showed that the SagA protein failed to degrade *S. aureus* and *B. cereus*, as observed by lysozymes (Table 2).

Table 2. Muramidase activity of SagA on *O*-acetylated PGNs

Strain	SagA
S. aureus RN4220	-
B. cereus ATCC 14579	-

The DAP-binding site

The *St*TtsA structure contained a DAP molecule in a small pocket in the C-terminal domain, far from the substrate-binding site (Geiger et al., 2020). SagA also has the corresponding DAP binding site surrounded by α7 and its flanking loop. The atomic coordinates of the backbone atoms (Val113, Gly115, and Lys117) and the side chains (Asp111 and Thr118) for the DAP binding site fit well between SagA and *St*TtsA (Fig. 5A).

To investigate the role of DAP binding in the catalysis of SagA, we compared the muramidase activities of SagA in the presence and absence of DAP. *M. lysodeikticus* cells were used for Lys-type PGN as substrates of SagA, and *B. subtilis* cells were used for DAP-type PGN. The addition of DAP reduced the SagA activity on Lys-type PGN, while the SagA activity on DAP-type PGN was not changed at an even higher concentration of DAP (Figs. 5B and 5C). In contrast to SagA, HEWL was not inhibited by the addition of DAP. Our findings suggest that the DAP binding of SagA is involved in Lys-type PGN degradation catalysis. Blocking the DAP binding site inhibited the hydrolysis of Lys-type PGN by SagA. Regarding DAP-type PGN, DAP binding is also crucial for recognizing DAP-type PGN, even though the addition of DAP did not affect the hydrolysis activity of SagA. We expected that the free DAP molecule could not complete the DAP moiety in the PGN bound in SagA.

The DAP binding site is approximately 29 Å apart from the substrate-binding site. In molecular modeling, we extended the bound PGN fragment to the DAP binding site by adding two PGN-repeating units (Fig. 5D). Thus, molecular docking indicates that the DAP binding site is interconnected in potentiation of PGN binding. The DAP binding of SagA might provide the collection or grabbing of the substrate PGN chain, which could be a molecular basis for higher activity than HEWL for DAP-type PGN.

Crystal structures and function of PhiA

Previous cell-based assays presented PhiA as a direct SagA inhibitor (Del Giudice et al., 2019). Moreover, the PhiA gene contains an MliC/PliC domain exhibiting a strong inhibitory effect on mammalian lysozymes (Del Giudice et al., 2019). Thus, the proposed function of PhiA is very plausible even though biochemical evidence is lacking. To confirm the role of PhiA, we noted the updated PhiA open reading frame starting at Met74 of the original entity (WP_002965354). The updated open reading frame was predicted to have a possible signal sequence for secretion to the periplasmic space at residue 60 or 62. To confirm the prediction, we expressed the new PhiA open reading frame with the entire N-terminal sequence in the *E. coli* system. The expressed PhiA protein was localized in the periplasmic space, and N-terminal amino acid sequencing revealed that residues 1-60 or -62 were cleaved off in the mature forms (Fig. 6A). These findings demonstrated that PhiA has a cleavable signal sequence for secretion to the periplasmic space, as predicted.

We determined the crystal structure of PhiA at 2.0 Å resolution to structurally analyze PhiA. The protomer of PhiA has

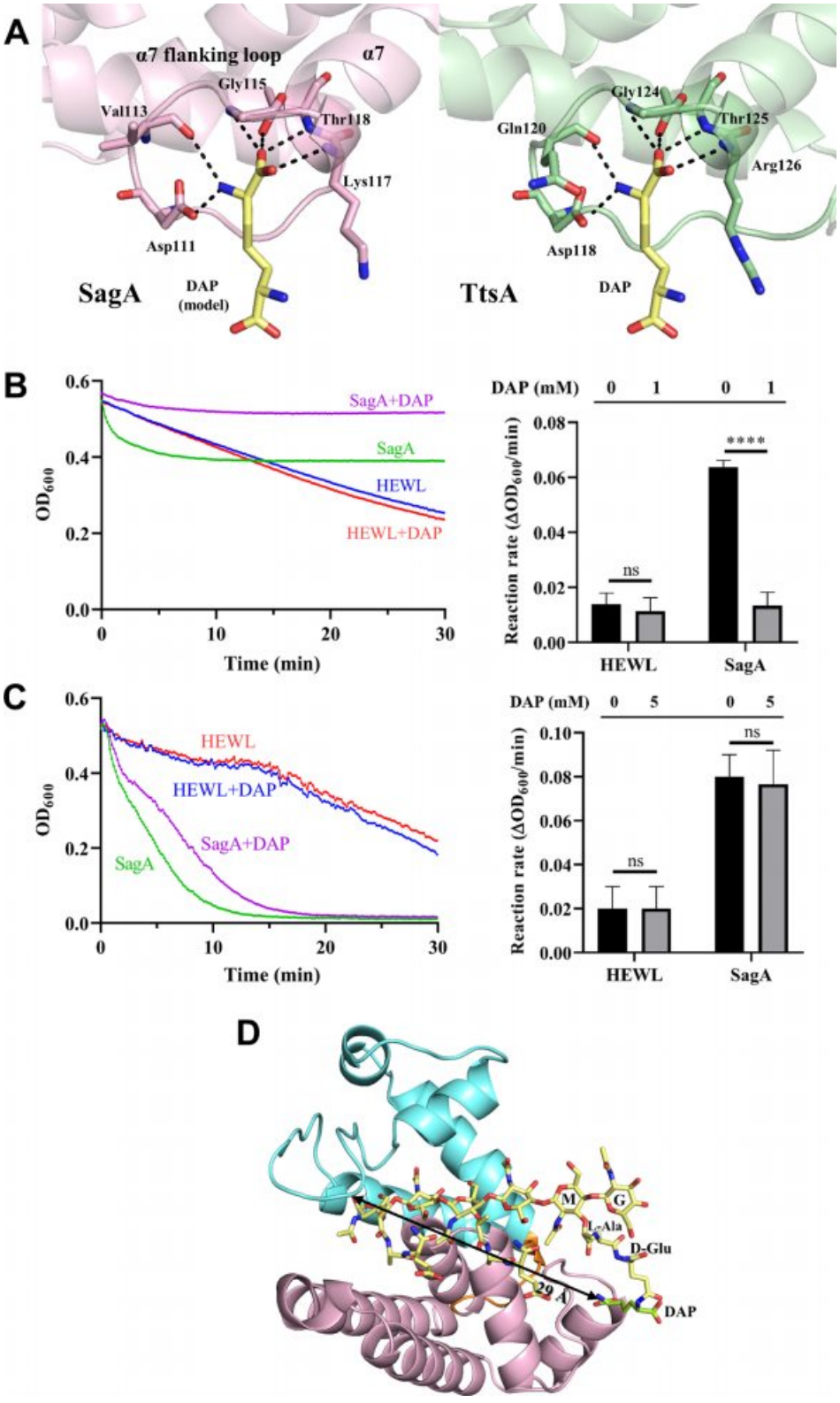

Fig. 5. DAP binding site of SagA and its effect on activity. (A) Docking model of SagA with DAP (left panel). α7 and its flanking loop of SagA (left panel, pink) are shown in the cartoon representation. The right panel presents the DAP-binding site of TtsA (green) shown in cartoon representation. The DAP (yellow) and the DAP-interacting residues of SagA and TtsA are shown in the stick model. (B) Effect of DAP addition on Lys-type PGN. The left panel indicates the turbidimetric changes in the HEWL- or SagA-treated *M. lysodeikticus* cells in the presence and absence of DAP. The right panel is the initial reaction rates of the turbidimetric changes (left panel). These results were produced from three independent experiments. Values are presented as mean ± SD. (C) Effect of DAP addition on DAP-type PGN. The left panel shows the turbidimetric changes in the HEWL- or SagA-treated *B. subtilis* cells in the presence and absence of DAP (left panel). The right panel is the initial reaction rates of HEWL and SagA from turbidimetric changes (left panel). These results were produced from three independent experiments. Values are presented as mean ± SD. ns, not significant. ****$P < 0.0001$. (D) Molecular model of SagA with extended PGN repeating units from the substrate-binding site to the DAP-binding site. The overall structure of the SagA protein is shown in the ribbon representations. The modeled PGN repeating units are shown in the stick model. The linked DAP molecule is highlighted in green. The distance between the substrate-binding site and the DAP-binding site is indicated.

a flattened β-barrel structure that consists of eight antiparallel β-strands, which is the typical structural fold of MliC and PliC (Fig. 6B). The β-barrel of PhiA is stabilized by the disulfide bonds Cys76 and Cys154. PhiA formed a stable tetramer both in solution and crystals, different from monomeric or dimeric PliC or MliC (Figs. 6A and 6D) (Leysen et al., 2011; Um et al., 2013; Yum et al., 2009). The SGxxY motif is conserved among MliC and PliC for binding to the active site of

lysozymes, as observed in the complex structures (Um et al., 2013; Yum et al., 2009). However, the PhiA structure did not contain the SGxxY motif on the primary structure or its equivalent motif at any protruding PhiA loop. The exposed hydroxy group of Ser in the SGxxY motif was critical for the interaction with the catalytic residues of the lysozymes in MliC and PliC. However, any corresponding structural feature was not found in PhiA in the structural superposition of PhiA on the PliC-human lysozyme complex structure (Fig. 6C).

We tested the inhibitory function of PhiA with the purified PhiA and SagA proteins. We failed to observe any direct binding or inhibitory function of PhiA with SagA and HEWL. The absence of the corresponding SGxxY motif might account for the lack of PhiA inhibitory function. Thus, our findings suggest that the inhibitory function of PhiA might act indirectly on SagA.

DISCUSSION

We determined the crystal structure of the muramidase SagA from *B. abortus* to be a clamp-like structure between the N-terminal hydrolase domain and the C-terminal PGN-binding domain. The mobile N-terminal hydrolase domain positions to the sessile bonds of PGN with the catalytic residues in the flexible loop, while the C-terminal PGN binding domain firmly holds the PGN unit mostly via van der Waals interactions. This molecular arrangement is reminiscent of the hammer-and-anvil tactic. The overall structural arrangement was similar to that of the T4 lysozyme. The bound PGN repeating unit provided structural details on the recognition of PGN.

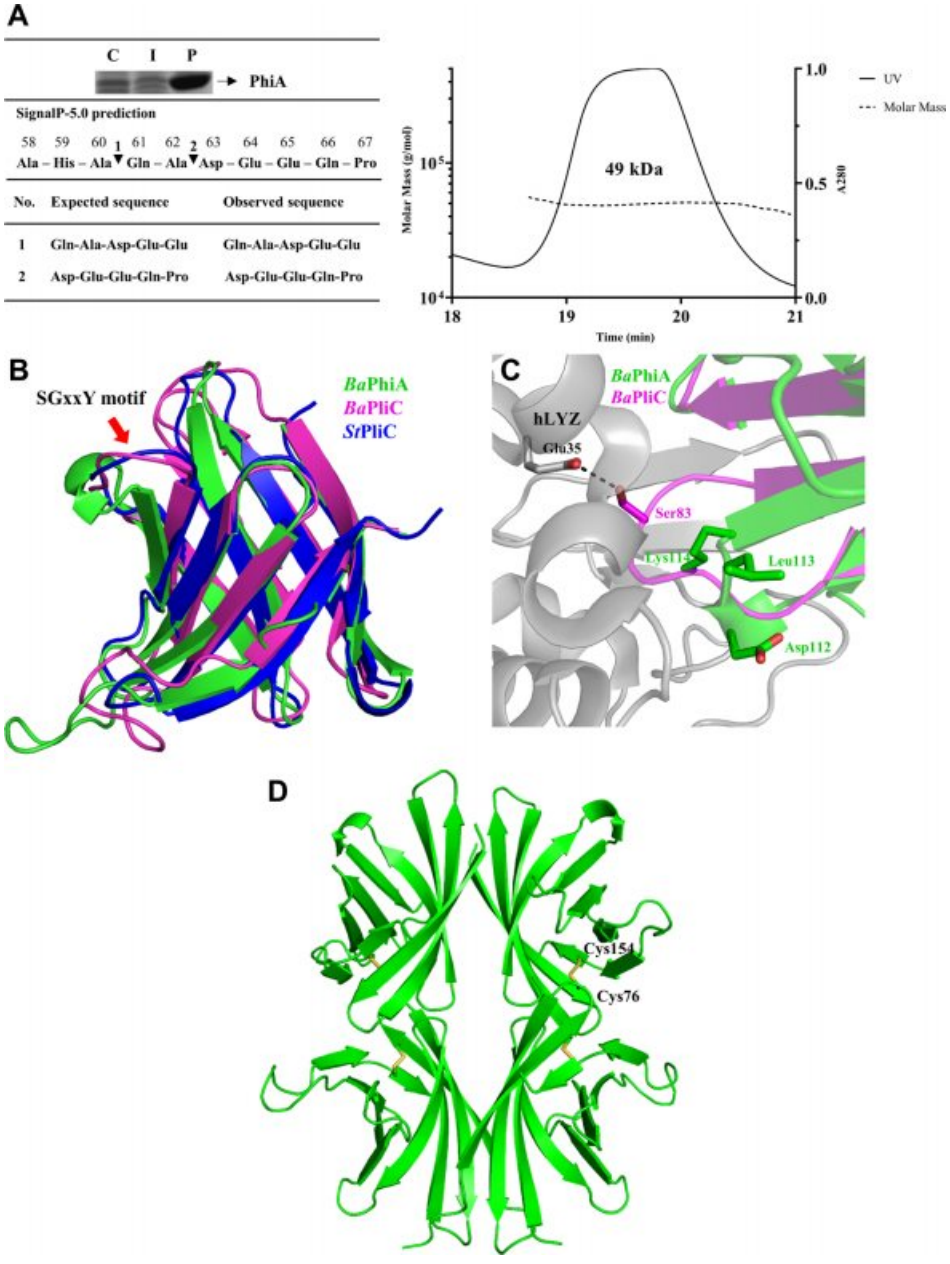

Fig. 6. Crystal structure and functional implications of PhiA. (A) SDS-PAGE analysis of fractionation of the recombinant PhiA protein in the *E. coli* system (left). C, cytoplasmic fraction; I, insoluble fraction; P, periplasmic fraction. The predicted cleavage sites of PhiA are indicated by arrows. Edman degradation of the expressed protein in the periplasm revealed equal probabilities of QADEE and DEEQP sequences. The SEC-MALS profile of PhiA is shown in the right panel, indicating the homotetrameric arrangement. (B) The structural superposition of *B. abortus* PhiA (*Ba*PhiA, green), *B. abortus* PliC (*Ba*PliC, magenta), and *S.* Typhimurium PliC (*St*PliC, blue) is shown in the ribbon representations. The SGxxY motif of PliC proteins is indicated by the red arrow. (C) The structural superposition of *B. abortus* PhiA (*Ba*PhiA, green), and *B. abortus* PliC (*Ba*PliC, magenta)-human lysozyme (hLYZ, grey) complex. The Ser83 of *Ba*PliC and Glu35 of hLYZ are shown in the stick model. The hydrogen bonds are indicated by the dotted line. The corresponding residues of *Ba*PhiA to SGxxY motif are shown in the stick model. (D) The tetrameric arrangement of PhiA is shown in the ribbon representations. Disulfide bonds of each protomer are shown in the stick models.

Comparison to the PGN-free *St*TtsA structure proposed the substrate-dependent hinge motion of the flap-like N-terminal domain. The structural comparison of SagA to the T4 lysozyme further suggested the closing of the loop containing the Glu, Asp, and Thr residues for catalysis toward the target atoms of the substrate. Thus, our findings indicate that the catalytic mechanism is shared with the T4 lysozyme.

Similar to mammalian lysozymes, SagA has muramidase activity on unmodified PGNs. Notably, SagA showed higher activity on DAP-type PGN than HEWL. This observation is expected because SagA works on the DAP-type PGN in the *Brucella* cell wall. However, SagA failed to digest Lys-type PGN completely by the product-inhibition mode. Moreover, the exogenous soluble DAP significantly inhibited the activity of SagA on Lys-type PGN unlike HEWL. Thus, our results suggest that SagA is specialized on the complete digestion of DAP-type PGN.

We also determined the crystal structure of PhiA from *B. abortus*, previously suggested as a direct inhibitor of SagA. Although the PhiA structure showed a similar fold to the MliC/PliC family proteins inhibiting lysozymes, the binding motif for inhibiting lysozymes was not present in PhiA. Since we could not observe any interaction between PhiA and SagA or HEWL, we speculate that it would modulate the activity of SagA in a different mode. It is also puzzling why the SagA/PhiA system is different from the lysozyme/MliC system. We presume that this difference might result from the purpose of the inhibitory proteins. While MliC proteins are the global inhibitor of all the lysozyme molecules, PhiA should act on SagA under the spatial and temporal limitation.

The crystal structure of SagA did not cover the transmembrane region (residues 223-245) or the linker region (residues 175-222) between the C-terminal domain and the transmembrane region (Fig. 1A). We hypothesized that the full-length SagA protein is immobilized to the inner membrane by the transmembrane region in the periplasmic space. The autolytic activity of SagA would be confined within the length of this linker region. If the transmembrane region of SagA interacts with type IV secretion system (T4SS), the localized activity of SagA in the T4SS would be explained. Thus, the confined activity of SagA would be crucial in preventing the further and unnecessary breakdown of the PGN layer.

Lysozymes have been employed to defend against bacteria in blood, tears, and many other body fluids (Hankiewicz and Swierczek, 1974). Due to its antimicrobial effect, lysozymes have been used as food or feed additives to control bacteria. However, many pathogenic gram-negative bacteria have natural inhibitory proteins to confer lysozyme resistance to the bacteria (Abergel et al., 2007; Callewaert et al., 2008; Monchois et al., 2001). Its limited antimicrobial efficacy against gram-negative bacteria restricts its application in the food industry. However, SagA showed higher muramidase activity than HEWL against DAP-type PGN (Fig. 4A). Furthermore, various lysozyme inhibitors from gram-negative bacteria will not inhibit the activity of SagA due to the entirely different primary and 3D structures between SagA and mammalian lysozymes. Thus, SagA has potential as a feed additive to control contaminated bacteria.

In conclusion, this study revealed high-resolution structures of SagA and PhiA. We analyzed the biochemical characteristics of SagA and suggested its substrate-binding mode. These findings have implications for the role of PhiA and the molecular basis for the SagA-PhiA system of *B. abortus*. The development of an inhibitor of SagA based on structural studies may further contribute to controlling brucellosis by attenuating T4SS, the major virulence factor of *Brucella*.

Note: Supplementary information is available on the Molecules and Cells website (www.molcells.org).

ACKNOWLEDGMENTS

This research was supported by Agriculture, Food, and Rural Affairs Convergence Technologies Program for Educating Creative Global Leader (710012-03-1-HD120). This research was also supported by the Bio & Medical Technology Development Program of the National Research Foundation (NRF) funded by the Korean government (MSIT) (NRF-2017M3A9F6029755). We made use of beamlines 5C and 11C at the Pohang Accelerator Laboratory (Pohang, Republic of Korea). This work was also supported by the BK21 Plus Program of the Department of Agricultural Biotechnology, Seoul National University, Seoul, Korea.

AUTHOR CONTRIBUTIONS

Y.H. and N.C.H. designed the research. Y.H., Y.B., C.L., and N.K. conceived and performed experiments. J.A., S.R., and N.C.H. provided expertise and feedback. Y.H. and N.C.H. wrote the manuscript, and N.C.H. secured funding.

CONFLICT OF INTEREST

The authors have no potential conflicts of interest to disclose.

ORCID

Yongseong Hyun https://orcid.org/0000-0002-4731-8492
Yeongjin Baek https://orcid.org/0000-0001-5119-1829
Chanyoung Lee https://orcid.org/0000-0002-4102-6528
Nayeon Ki https://orcid.org/0000-0003-3225-1413
Jinsook Ahn https://orcid.org/0000-0002-4175-5181
Sangryeol Ryu https://orcid.org/0000-0001-5812-3394
Nam-Chul Ha https://orcid.org/0000-0003-4813-748X

REFERENCES

Abergel, C., Monchois, V., Byrne, D., Chenivesse, S., Lembo, F., Lazzaroni, J.C., and Claverie, J.M. (2007). Structure and evolution of the Ivy protein family, unexpected lysozyme inhibitors in Gram-negative bacteria. Proc. Natl. Acad. Sci. U. S. A. *104*, 6394-6399.

Adams, P.D., Afonine, P.V., Bunkóczi, G., Chen, V.B., Davis, I.W., Echols, N., Headd, J.J., Hung, L.W., Kapral, G.J., Grosse-Kunstleve, R.W., et al. (2010). PHENIX: a comprehensive Python-based system for macromolecular structure solution. Acta Crystallogr. D Biol. Crystallogr. *66*, 213-221.

Alvarez-Martinez, C.E. and Christie, P.J. (2009). Biological diversity of prokaryotic type IV secretion systems. Microbiol. Mol. Biol. Rev. *73*, 775-808.

Archambaud, C., Salcedo, S.P., Lelouard, H., Devilard, E., de Bovis, B., Van Rooijen, N., Gorvel, J.P., and Malissen, B. (2010). Contrasting roles of macrophages and dendritic cells in controlling initial pulmonary *Brucella* infection. Eur. J. Immunol. *40*, 3458-3471.

Callewaert, L., Aertsen, A., Deckers, D., Vanoirbeek, K.G., Vanderkelen, L.,

Van Herreweghe, J.M., Masschalck, B., Nakimbugwe, D., Robben, J., and Michiels, C.W. (2008). A new family of lysozyme inhibitors contributing to lysozyme tolerance in gram-negative bacteria. PLoS Pathog. *4*, e1000019.

Del Giudice, M.G., Romani, A.M., Ugalde, J.E., and Czibener, C. (2019). PhiA, a peptidoglycan hydrolase inhibitor of *Brucella* involved in the virulence process. Infect. Immun. *87*, e00352-19.

Del Giudice, M.G., Ugalde, J.E., and Czibener, C. (2013). A lysozyme-like protein in *Brucella abortus* is involved in the early stages of intracellular replication. Infect. Immun. *81*, 956-964.

Dijkstra, A.J. and Keck, W. (1996). Peptidoglycan as a barrier to transenvelope transport. J. Bacteriol. *178*, 5555-5562.

Emsley, P. and Cowtan, K. (2004). Coot: model-building tools for molecular graphics. Acta Crystallogr. D Biol. Crystallogr. *60*(Pt 12 Pt 1), 2126-2132.

Geiger, T., Lara-Tejero, M., Xiong, Y., and Galan, J.E. (2020). Mechanisms of substrate recognition by a typhoid toxin secretion-associated muramidase. Elife *9*, e53473.

Hankiewicz, J. and Swierczek, E. (1974). Lysozyme in human body fluids. Clin. Chim. Acta *57*, 205-209.

Hodak, H. and Galan, J.E. (2013). A *Salmonella* Typhi homologue of bacteriophage muramidases controls typhoid toxin secretion. EMBO Rep. *14*, 95-102.

Hueck, C.J. (1998). Type III protein secretion systems in bacterial pathogens of animals and plants. Microbiol. Mol. Biol. Rev. *62*, 379-433.

Hyun, Y., Ahn, J., Baek, Y., Xu, Y., and Ha, N.C. (2020). Purification, crystallization, and preliminary analysis of the lysozyme-like enzyme SagA from *Brucella abortus*. Biodesign *8*, 64-67.

Kanonenberg, K., Schwarz, C.K., and Schmitt, L. (2013). Type I secretion systems–a story of appendices. Res. Microbiol. *164*, 596-604.

Koraimann, G. (2003). Lytic transglycosylases in macromolecular transport systems of Gram-negative bacteria. Cell. Mol. Life Sci. *60*, 2371-2388.

Korotkov, K.V., Sandkvist, M., and Hol, W.G. (2012). The type II secretion system: biogenesis, molecular architecture and mechanism. Nat. Rev. Microbiol. *10*, 336-351.

Kuroki, R., Weaver, L.H., and Matthews, B.W. (1993). A covalent enzyme-substrate intermediate with saccharide distortion in a mutant T4 lysozyme. Science *262*, 2030-2033.

Kuroki, R., Weaver, L.H., and Matthews, B.W. (1999). Structural basis of the conversion of T4 lysozyme into a transglycosidase by reengineering the active site. Proc. Natl. Acad. Sci. U. S. A. *96*, 8949-8954.

Lasica, A.M., Ksiazek, M., Madej, M., and Potempa, J. (2017). The type IX secretion system (T9SS): highlights and recent insights into its structure and function. Front. Cell. Infect. Microbiol. *7*, 215.

Leysen, S., Van Herreweghe, J., Callewaert, L., Heirbaut, M., Buntinx, P., Michiels, C., and Strelkov, S. (2011). Molecular basis of bacterial defense against host lysozymes: X-ray structures of periplasmic lysozyme inhibitors PliI and PliC. J. Mol. Biol. *405*, 1233-1245.

Matthews, B. and Remington, S. (1974). The three dimensional structure of the lysozyme from bacteriophage T4. Proc. Natl. Acad. Sci. U. S. A. *71*, 4178-4182.

McCoy, A.J., Grosse-Kunstleve, R.W., Adams, P.D., Winn, M.D., Storoni, L.C., and Read, R.J. (2007). Phaser crystallographic software. J. Appl. Crystallogr. *40*, 658-674.

Monchois, V., Abergel, C., Sturgis, J., Jeudy, S., and Claverie, J.M. (2001). *Escherichia coli* ykfE ORFan gene encodes a potent inhibitor of C-type lysozyme. J. Biol. Chem. *276*, 18437-18441.

Myeni, S., Child, R., Ng, T.W., Kupko, J.J., 3rd, Wehrly, T.D., Porcella, S.F., Knodler, L.A., and Celli, J. (2013). *Brucella* modulates secretory trafficking via multiple type IV secretion effector proteins. PLoS Pathog. *9*, e1003556.

Notredame, C., Higgins, D.G., and Heringa, J. (2000). T-Coffee: a novel method for fast and accurate multiple sequence alignment. J. Mol. Biol. *302*, 205-217.

Otwinowski, Z. and Minor, W. (1997). [20] Processing of X-ray diffraction data collected in oscillation mode. Methods Enzymol. *276*, 307-326.

Pappas, G., Papadimitriou, P., Akritidis, N., Christou, L., and Tsianos, E.V. (2006). The new global map of human brucellosis. Lancet Infect. Dis. *6*, 91-99.

Pei, J. and Grishin, N.V. (2005). COG3926 and COG5526: a tale of two new lysozyme-like protein families. Protein Sci. *14*, 2574-2581.

Puigbo, P., Guzman, E., Romeu, A., and Garcia-Vallve, S. (2007). OPTIMIZER: a web server for optimizing the codon usage of DNA sequences. Nucleic Acids Res. *35*(Web Server issue), W126-W131.

Pukatzki, S., McAuley, S.B., and Miyata, S.T. (2009). The type VI secretion system: translocation of effectors and effector-domains. Curr. Opin. Microbiol. *12*, 11-17.

Robert, X. and Gouet, P. (2014). Deciphering key features in protein structures with the new ENDscript server. Nucleic Acids Res. *42*(Web Server issue), W320-W324.

Scheurwater, E., Reid, C.W., and Clarke, A.J. (2008). Lytic transglycosylases: bacterial space-making autolysins. Int. J. Biochem. Cell Biol. *40*, 586-591.

Stojkovic, E.A. and Rothman-Denes, L.B. (2007). Coliphage N4 *N*-acetylmuramidase defines a new family of murein hydrolases. J. Mol. Biol. *366*, 406-419.

Terwilliger, T.C., Adams, P.D., Read, R.J., McCoy, A.J., Moriarty, N.W., Grosse-Kunstleve, R.W., Afonine, P.V., Zwart, P.H., and Hung, L.W. (2009). Decision-making in structure solution using Bayesian estimates of map quality: the PHENIX AutoSol wizard. Acta Crystallogr. D Biol. Crystallogr. *65*, 582-601.

Um, S.H., Kim, J.S., Kim, K., Kim, N., Cho, H.S., and Ha, N.C. (2013). Structural basis for the inhibition of human lysozyme by PliC from *Brucella abortus*. Biochemistry *52*, 9385-9393.

Yum, S., Kim, M.J., Xu, Y., Jin, X.L., Yoo, H.Y., Park, J.W., Gong, J.H., Choe, K.M., Lee, B.L., and Ha, N.C. (2009). Structural basis for the recognition of lysozyme by MliC, a periplasmic lysozyme inhibitor in Gram-negative bacteria. Biochem. Biophys. Res. Commun. *378*, 244-248.